Geochemistry, Geophysics, Geosystems

RESEARCH ARTICLE
10.1029/2019GC008819

Constraints on the Rheology of the Lithosphere From Flexure of the Pacific Plate at the Hawaiian Islands

Ashley Bellas[1], Shijie Zhong[1], and Anthony Watts[2]

[1]Department of Physics, University of Colorado Boulder, Boulder, CO, USA, [2]Department of Earth Sciences, Oxford University, Oxford, UK

Key Points:
- Lithospheric rheology from laboratory experiments is formulated in viscoelastic loading models and tested against observations of flexure
- Current laboratory-derived flow laws underpredict observations of flexure, but a modest reduction in activation energy produces good agreement
- Thermal rejuvenation by a plume alters only the deep lithosphere and has negligible impact on flexure

Supporting Information:
- Supporting Information S1

Correspondence to:
A. Bellas,
ashley.bellas@colorado.edu

Citation:
Bellas, A., Zhong, S., & Watts, A. (2020). Constraints on the rheology of the lithosphere from flexure of the Pacific Plate at the Hawaiian Islands. *Geochemistry, Geophysics, Geosystems*, *21*, e2019GC008819. https://doi.org/10.1029/2019GC008819

Received 13 NOV 2019
Accepted 18 JAN 2020
Accepted article online 22 JAN 2020

Abstract The rheology of oceanic lithosphere is important to our understanding of mantle dynamics and to the emergence and manifestations of plate tectonics. Data from experimental rock mechanics suggest rheology is dominated by three different deformation mechanisms including frictional sliding, low-temperature plasticity, and high-temperature creep, from shallow depths at relatively cold temperatures to large depths at relatively high temperatures. However, low-temperature plasticity is poorly understood. This study further constrains low-temperature plasticity by comparing observations of flexure at the Hawaiian Islands to predictions from 3-D viscoelastic loading models with a realistic lithospheric rheology of frictional sliding, low-temperature plasticity, and high-temperature creep. We find that previously untested flow laws significantly underpredict the amplitude and overpredict the wavelength of flexure at Hawaii. These flow laws can, however, reproduce observations if they are weakened by a modest reduction (25–40%) in the plastic activation energy. Lithospheric rheology is strongly temperature dependent, and so we explore uncertainties in the thermal structure with different conductive cooling models and convection simulations of plume-lithosphere interactions. Convection simulations show that thermal erosion from a plume only perturbs the lithospheric temperature significantly at large depths so that when it is added to the thermal structure, it produces a small increase in deflection. In addition, defining the temperature profile by the cooling plate model produces only modest weakening relative to the cooling half-space model. Therefore, variation of the thermal structure does not appear to be a viable means of bringing laboratory-derived flow laws for low-temperature plasticity into agreement with geophysical field observations and modeling.

Plain Language Summary Volcanic eruptions continually build the Hawaiian Island chain. The islands impose stresses on the Pacific plate that bends in response to their weight. The degree to which the plate bends is controlled by the plate's strength. The strength of tectonic plates on Earth has implications for the long-term evolution of the entire planet. We are thus motivated to constrain the strength of the Pacific plate by comparing observations of the flexure of the top of ocean crust to predictions from computer simulations. The computer simulations incorporate flow laws from laboratory experiments on constituent minerals. We find that laboratory-derived flow laws underpredict the flexure and hence overpredict the strength of the plate. The flow laws make predictions consistent with observations, however, if we apply a modest variation to the sensitivity to changes in temperature. Meanwhile, the source of volcanic activity at Hawaii is a mantle plume composed of buoyant material that flows from the core-mantle boundary to the surface. We test whether the plume significantly warms and erodes the plate. A plume only effects the deepest part of the plate, while the shallower portion of the plate remains strong and so has little impact on the flexure.

1. Introduction

Deformation under stress is governed by the rheology of the stressed material. The main mechanisms that govern deformation in Earth's mantle at low, intermediate, and high temperatures are frictional sliding, low-temperature plasticity (LTP), and high-temperature creep, respectively (Figure 1a). The strongest portion is the upper thermal boundary layer, or lithosphere, due to its low temperature. Because of its high strength, the lithosphere has a controlling effect on the evolution and dynamics of Earth, including the emergence and manifestations of plate tectonics.

The geoscience community has historically investigated rheology using surface observations such as gravity, geoid, and static and dynamical models of flexure and laboratory experiments on constituent mantle

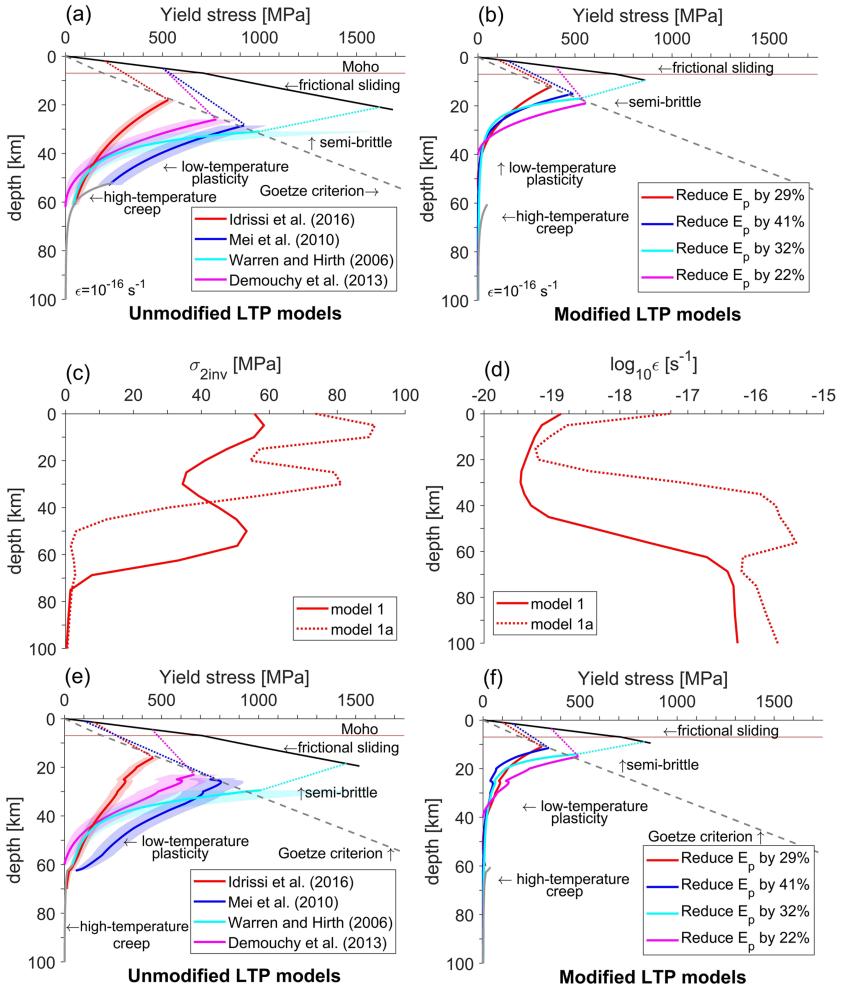

Figure 1. Modified from Mei et al. (2010), (a) the yield-strength envelope (YSE) is determined from the flow laws for frictional sliding, low-temperature plasticity, and high-temperature creep. The medium yields by the weakest deformation mechanism at the given conditions when the local stress exceeds the yield stress. The YSE thus represents the maximum possible stress profile for the given strain rate. The temperature profile is consistent with 90 Myr old oceanic lithosphere. The shaded regions show the appreciable range in yield strength corresponding to 5% variation in plastic activation energy, E_p. To solve the yield strength of frictional sliding, the imposed minimum principal stress is lithostatic, which is consistent with thrust faults and maximum fault strength (Sibson, 1974; Zoback & Townend, 2001). The poorly understood semibrittle regime is linearly interpolated between the yield strength of low-temperature plasticity (LTP) at the Goetze criterion and frictional sliding at the depth for which frictional strength is 5 times the strength of LTP (Kohlstedt et al., 1995). (b) The YSE predicted by LTP flow laws that have been weakened by a reduction in plastic activation energy. (c) The horizontally averaged stress and (d) strain rate within a 250 km lateral radius of the Big Island from Models 1 and 1a with LTP from Idrissi et al. (2016). The stress from models is significantly less than the YSE. The YSE for unmodified (e) and modified (f) LTP flow laws computed with the depth-varying strain rate taken from Model 1a (d).

minerals such as olivine. In the case of laboratory experiments, high-temperature creep is the best understood. This is, in part, due to the relative ease of performing experiments on warmer ($T > 1000$ °C) rock samples and, in part, due to abundant field observables that constrain high-temperature creep rheology, for example, postseismic deformation (Freed et al., 2010), postglacial rebound (Peltier, 1976), and dynamic topography and the geoid (Hager & Richards, 1989). A high level of understanding is corroborated by compelling consistency between the real Earth and predictions from geodynamic models which incorporate results from surface observations and experimental rock mechanics, for example, the long-wavelength convective structure and associated supercontinent cycle (Zhong et al., 2007).

The laboratory study of Byerlee (1978) demonstrates that the strength of frictional sliding on faults is largely independent of rock type, surface roughness, and temperature but rather is governed by a yield stress that is

proportional to a frictional coefficient and normal stress on the fault. Byerlee (1978) reports the frictional coefficient $\mu_f = 0.6–0.85$ which is generally consistent with in situ borehole measurements that suggest $\mu_f = 0.6$ (Zoback & Townend, 2001) and with the modeling the flexure caused by the emplacement of volcanic loads on oceanic crust in the plate interiors (e.g., Hawaii) that suggest $\mu_f \geq 0.25$ (Zhong & Watts, 2013).

LTP remains the least understood mechanism relevant to deformation of the lithosphere due to difficulties in performing experiments and a lack of relevant field observations. Two significant difficulties are (1) to perform experiments on mantle rocks at conditions for which LTP dominates deformation (i.e., temperature, stress, and deformation rate) and (2) to extrapolate over many orders of magnitude in strain rate from laboratory to lithospheric conditions (i.e., ~10^{-16} s^{-1} in the field compared to ~10^{-6} s^{-1} in the laboratory). In the current literature, there is a significant disagreement between different laboratory studies and between laboratory results and geodynamic models of the observations of flexure (Figure 1a). For example, the low-temperature plastic flow laws from experimental studies may vary in mathematical form and in parameters including the Peierls stress from 3.8 to 15 GPa and the activation energy from 320 to 566 kJ/mol (Demouchy et al., 2013; Idrissi et al., 2016; Mei et al., 2010; Warren & Hirth, 2006).

Geodynamical modeling offers an opportunity to calibrate experimental LTP flow laws to surface observables at strain rates not feasible in the laboratory. Volcano load-induced deformation at the Hawaiian Islands provides one of the best opportunities to test lithospheric rheology, because robust observations are available, where both the load and response of the plate are constrained by seismic reflection profiles, gravity anomaly, and topography data (Watts & ten Brink, 1989). Zhong and Watts (2013) found that laboratory-derived LTP flow laws (e.g., Mei et al., 2010) must be weakened by a preexponential factor of 10^8 in order to reproduce the amplitude and wavelength of the observed flexure and depth distribution of seismicity at Hawaii. This has led to new experimental studies on the cause of the discrepancy between the field-based and laboratory studies on the LTP flow laws (Idrissi et al., 2016; Kumamoto et al., 2017). However, there are several limitations in the approach of Zhong and Watts (2013) that require further investigation.

First, Zhong and Watts (2013) only vary the preexponential factor of LTP flow laws and keep other parameters unchanged. We note that each parameter in laboratory-derived flow laws may change the fit to observational data. Therefore, it is important to consider varying other flow law parameters with different functional dependence in strength, such as the activation energy to which the flow laws are more sensitive (Jain et al., 2017). Second, Zhong and Watts (2013) only consider a cooling half-space cooling model for the lithosphere in the Hawaiian region, thereby ignoring the cooling plate model (e.g., Parsons & Sclater, 1977; Stein & Stein, 1992), and possible thermal rejuvenation associated with the Hawaiian plume (Detrick & Crough, 1978; Guest et al., 2018). Although significant thermal rejuvenation of the Pacific oceanic lithosphere at the Hawaiian Islands is inconsistent with the heat flux measurements (von Herzen et al., 1989), the inferred elastic thickness (e.g., Wessel, 1993; Watts & Zhong, 2000), and observations of surface wave dispersion (Ritzwoller et al., 2004; Woods et al., 1991), it is nevertheless important to test the potential effects of different thermal structures on the observations of flexure.

The purpose of this paper is to test the effects of activation energy and lithospheric thermal structure on the lithospheric response to volcanic loading and seek the range of model parameters that are required to fit the observations of flexure at Hawaii. We also test a different set of low-temperature plastic flow laws (Demouchy et al., 2013; Idrissi et al., 2016; Warren & Hirth, 2006) than those previously tested by Zhong and Watts (2013) (e.g., Evans & Goetze, 1979; Katayama & Karato, 2008; Mei et al., 2010; Raterron et al., 2004), which may be weaker for the same stress. To quantitatively address the effects of plume-lithosphere interaction on the thermal structure (i.e., thermal rejuvenation) and flexure, we formulate convection simulations with a plume and varying viscosity structure in the lithosphere (Ballmer et al., 2013; Ribe & Christensen, 1994; Zhong & Watts, 2002). The plume-induced temperature anomaly can then be added to the thermal structure of the lithosphere and the different flow laws used to calculate the equivalent elastic thickness and compared to the observations of flexure.

2. Description of the Viscoelastic Loading Model and the Convection Model for Plume-Lithosphere Interaction

This study is based on two independent sets of models. The first is a viscoelastic loading model that computes flexure and stress in response to a volcano load that has been emplaced on the surface of preexisting oceanic

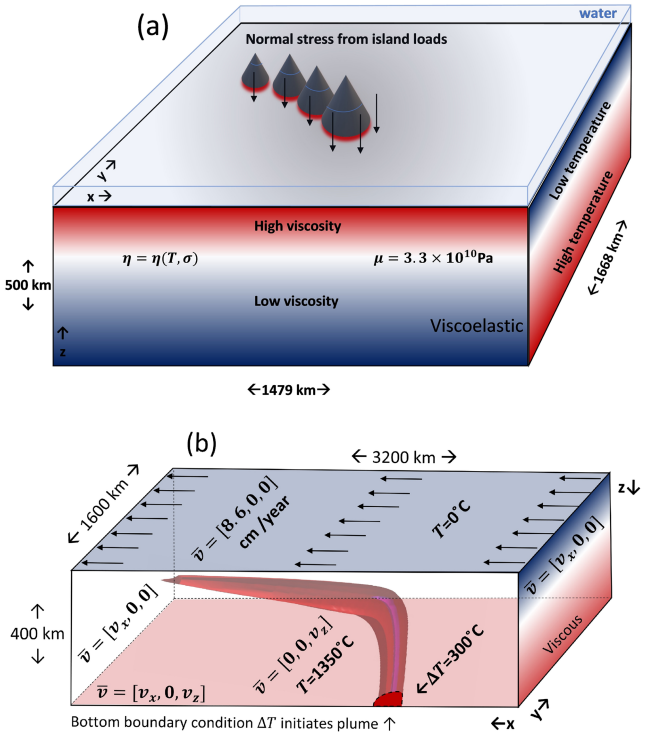

Figure 2. Cartoons of (a) the viscoelastic loading model and (b) the purely viscous thermal convection model with a plume. The loading model (a) accounts for infill by water as the plate deflects and infill by sediments when deflection exceeds the local inferred residual topography (Figure 3b). The convection model (b) simulates a plume that develops from a circular temperature anomaly of 300 K at the bottom boundary. The surface velocity is set to 8.6 cm/year, consistent with Pacific plate motion. The bottom, left, and right boundaries allow material to flow through, but there is no slip. The front and rear boundary conditions are free slip (or, equivalently, reflecting). A simple coordinate transformation brings the temperature anomaly from a plume into the reference frame of loading calculations.

crust in a plate interior and that varies both spatially and temporally (Figure 2a). The second is a mantle convection model for plume-lithosphere interaction (Figure 2b). The loading and convection models used here are nearly identical to those used in Zhong and Watts (2013) and Zhong and Watts (2002), respectively. Here we will discuss briefly these two models.

2.1. Hawaiian Volcanic Loads and Lithospheric Rheology

2.1.1. Governing Equations and Boundary Conditions

In the case of the crust and lithosphere response to volcano loading on the timescale of a few million years, both viscous and elastic rheology are relevant (e.g., >Watts & Zhong, 2000). The response of an incompressible viscoelastic medium can be expressed by the conservation of mass and momentum (e.g., Wu, 1992; Zhong & Watts, 2013)

$$u_{i,i} = 0, \tag{1}$$

$$\sigma_{ij,j} - (\rho_0 g u_3)_{,i} = 0, \tag{2}$$

where u_i is the displacement vector, σ_{ij} is the stress tensor, ρ_0 the ambient mantle density, g the acceleration due to gravity, and u_3 the vertical component of the displacement vector. The second term in equation (2) represents the restoring force at deformed density interfaces. We use notation such that $A_{,i}$ denotes the derivative with respect to x_i, and repeated indices are summed over.

Our loading model is a 3-D Cartesian box with dimensions of 1,479 km in x (east-west), 1,668 km in y (north-south), and 500 km in z (depth). This is consistent with a domain ranging from 12.5–27.5°N and 165–150°W (Zhong & Watts, 2013). The boundary conditions at the four vertical sidewalls and bottom boundary are free slip (Figure 2a). The top boundary is treated as a deformable, free surface subject to time-dependent loads, $\sigma_L(x, y, t)$ (i.e., the individual Hawaiian volcanoes)

$$\sigma_{ij} n_j = \sigma_L(x, y, t) n_i, \tag{3}$$

where n_i is the unit vector normal to the upper boundary. The details of the loads will be discussed later.

2.1.2. Lithospheric and Crust and Mantle Rheology Relevant to the Hawaiian Volcanic Loading Problem

For an incompressible Maxwellian medium, the stress tensor is given by (Zhong & Watts, 2013)

$$\sigma_{ij} + \frac{\eta}{\mu}\dot{\sigma}_{ij} = -p\delta_{ij} + 2\eta\dot{\epsilon}_{ij}, \tag{4}$$

where η is the viscosity, μ the shear modulus, p the pressure, and $\dot{\epsilon}_{ij}$ the strain rate tensor. The time derivative of stress term in equation (4) distinguishes this equation from purely viscous flow. An important time is given by the coefficient $\eta/\mu = \tau_M$, the Maxwell time. The Maxwell time is a measure of the timescale on which viscoelastic deformation occurs (i.e., viscoelastic relaxation of stresses). The strain rate tensor, $\dot{\epsilon}_{ij}$, accounts for both viscous and elastic deformation. We assume a simple model of elastic deformation in which the shear modulus, μ, is uniform.

Lithospheric and crust and mantle viscosity depend on deformation mechanisms that are highly nonlinear and stress and temperature dependent, according to laboratory studies (e.g., Kohlstedt et al., 1995). In the uppermost lithosphere, deformation occurs by frictional sliding, whereby failure is activated on preexisting faults when a certain yield stress is exceeded. The yield stress is empirically found to increase with depth following Byerlee's law (Figure 1a)

Table 1
Model Parameters

Parameter	Value
Mantle temperature (T_m)	1350 °C
Shear modulus (μ)	3.3×10^{10} Pa
Frictional coefficient (μ_f)	0.7
Thermal diffusivity (κ)	10^{-6} m^2/s
Gravitational acceleration (g)	9.8 m/s^2
Gas constant (R)	8.32 J/(mol K)
Mantle density (ρ_0)	3,330 kg/m^3
Crustal density (ρ_c)	2,800 kg/m^3
Water density (ρ_w)	1,030 kg/m^3
Rock infill density (ρ_{sd})	2,800 kg/m^3

High-temperature creep rheology	
Power law exponent (n)	3.5
Activation energy (E_c)	360 kJ/mol
Transition stress (σ_{trans})	3×10^5 Pa
Asthenospheric viscosity (η_0)	10^{20} Pa s

Low-temperature plastic rheology

Laboratory study	E_p (kJ/mol)	σ_p (GPa)	p	q	n	A
Idrissi et al. (2016)	566	3.8	½	2	0	1.0×10^6 s^{-1}
Mei et al. (2010)	320	5.9	½	1	2	1.4×10^{-7} s^{-1} MPa^{-2}
Warren and Hirth (2006)	470	—	—	0	8.5	2.4×10^{-7} s^{-1} MPa$^{-8.5}$
Demouchy et al. (2013)	450	15	½	2	0	1.0×10^6 s^{-1}

$$\tau = \mu_f \sigma_n + C_f, \tag{5}$$

where τ is the shear stress of failure, μ_f is the frictional coefficient, σ_n is the normal stress on the fault, and C_f is the strength of cohesion. The frictional coefficient $\mu_f = 0.7$ for all cases in this study.

As pressure, and hence normal stress, increases on a fault with depth, frictional sliding is suppressed. Conversely, as temperature increases with depth, the yield strength of LTP decreases, and it yields more readily (Figure 1a). The LTP flow law takes an exponential form (Evans & Goetze, 1979)

$$\dot{\epsilon} = A\sigma^n \exp\left(-\frac{E_p}{RT}\left(1-\left(\frac{\sigma}{\sigma_p}\right)^p\right)^q\right), \tag{6}$$

where $\dot{\epsilon}$ is the second invariant of the strain rate tensor, A is the preexponential factor, σ is the second invariant of the deviatoric stress tensor, n the stress exponent, E_p is the plastic activation energy, R the universal gas constant, T the temperature, σ_p the Peierls stress or dislocation glide resistance, and the exponents p and q control sensitivity to stress. The parameter values for various LTP flow laws tested in this study are listed in Table 1.

Laboratory studies suggest the onset of LTP is determined by the Goetze criterion (Figure 1a), which states that brittle deformation may activate only for differential stress larger than the normal stress (Kohlstedt & Mackwell, 2009), such that LTP dominates deformation once the yield strength is exceeded by lithostatic pressure. Temperature and pressure gradients in the lithosphere typically result in LTP-dominant deformation for temperatures ranging 400–800 °C (Figure 1a). In the volcano loading model, for $T < 800$ °C, whichever is weaker of frictional sliding and LTP controls the local deformation and defines the local effective viscosity.

Furthermore, laboratory studies report that when the yield strength of LTP is a factor of ~5 larger than that of frictional sliding, the semibrittle regime is activated (Kohlstedt et al., 1995; Figure 1a). Semibrittle deformation is poorly understood but may manifest itself as a combination of distributed brittle failure and plastic yielding. We do not include semibrittle deformation in our model, and this does not introduce significant error, because in the region for which semibrittle rheology is relevant, it is so strong that no appreciable

deformation is accommodated by the semibrittle mechanism on the timescale of Hawaiian volcano building (Zhong & Watts, 2013).

When temperatures are sufficiently high, deformation by high-temperature creep is activated. In this study, we set high-temperature creep as the dominant mechanism at temperatures higher than 800 °C. High-temperature creep is described by an exponential form following

$$\dot{\epsilon} = A\sigma^n \exp\left(-\frac{E_c}{RT}\right), \tag{7}$$

where A is the preexponential factor, the stress exponent n is set to either 1 or 3.5 for linear (diffusion) or nonlinear (dislocation) creep, respectively, both of which are implemented in a composite law, and E_c is the creep activation energy. From laboratory experiment, E_c is ~500 kJ/mol. However, we use E_c = 360 kJ/mol for all models in the present study to be consistent with field-based studies on sublithospheric small-scale convection (van Hunen et al., 2005). Irrespective, Zhong and Watts (2013) demonstrate that flexure is largely insensitive to high-temperature creep rheology for reasonable asthenospheric viscosity (10^{20}–s10^{22} Pa s). All parameter values are listed in Table 1.

Finally, the thermal structure has a controlling effect on the rheology. Zhong and Watts (2013) used a cooling half-space model to compute the temperature profile in the lithosphere

$$T = T_0 + \Delta T erf\left(\frac{z}{2\sqrt{\kappa t_s}}\right), \tag{8}$$

where *erf* is the error function, z is depth, t_s is the local age of the crust, and κ is the thermal diffusivity. In this study, we also test the effect of defining temperature by the plate model (Stein & Stein, 1992) and add a temperature perturbation to test the effects of plume-lithosphere interaction on flexure.

2.1.3. Observations of Flexure and the Loads at Hawaii

The deflection of the Pacific plate in the vicinity of the Hawaiian Islands is driven, we believe, by loading due to the emplacement of volcanic material on the preexisting surface of the oceanic crust. The loading history has been reconstructed by Zhong and Watts (2013), using the bathymetry corrected for thermal isostasy, sediments, and Hawaiian swell topography to isolate the loads from residual topography (Figure 3). The volcanoes considered have been built continuously over the last ~5 Myr, and we approximate the loading history into four stages for computational efficiency (Figure 3). As discussed in Zhong and Watts (2013), while the loading history in our model for the last 2 Myr is consistent with the observations, our model loading history for earlier times is condensed into a shorter time period for computational efficiency with no effect on deformation history and total deformation for the past million years for which the observations are compared.

The main observations used to constrain the model results are seismic refraction and reflection data, as acquired during the offshore/onshore refraction experiments of Zucca et al. (1982) and Zucca and Hill (1980) around Hawaii, the two-ship refraction experiment of Shor and Pollard (1964) near north Maui, and the two-ship multichannel reflection and refraction experiment of Watts et al. (1985) and Watts and ten Brink (1989) which intersected the Hawaiian ridge between Oahu and Molokai and Oahu and Kauai (Figure 3). The latter experiment, by Watts and ten Brink (1989), defined the top and base of the oceanic crust on either side of the ridge, and when corrected for thermal age, sediments, and swell topography, can be used as a constraint on the deformation of the crust due to volcano loading. The seismic data reveal that the crust is flexed downward by up to 4 km immediately below islands, with flexure decreasing away from the islands toward the flexural bulge comprising the North and South Hawaiian arches (e.g., black circles in Figure 4b).

2.1.4. Modeling

Zhong and Watts (2013) describe how the governing equations with viscoelastic rheology and three different deformation mechanisms can be solved numerically using a 3-D finite element code CitcomSVE, which was originally designed to solve glacial isostatic adjustment problems (Zhong et al., 2003). Here, we use the same methods as described in Zhong and Watts (2013). The deformation is driven by the volcano loading history, as discussed above. The model predicts the time-dependent flexure, deformation, and stress field. The predicted flexure at the present day based on models with different rheological parameters is then compared

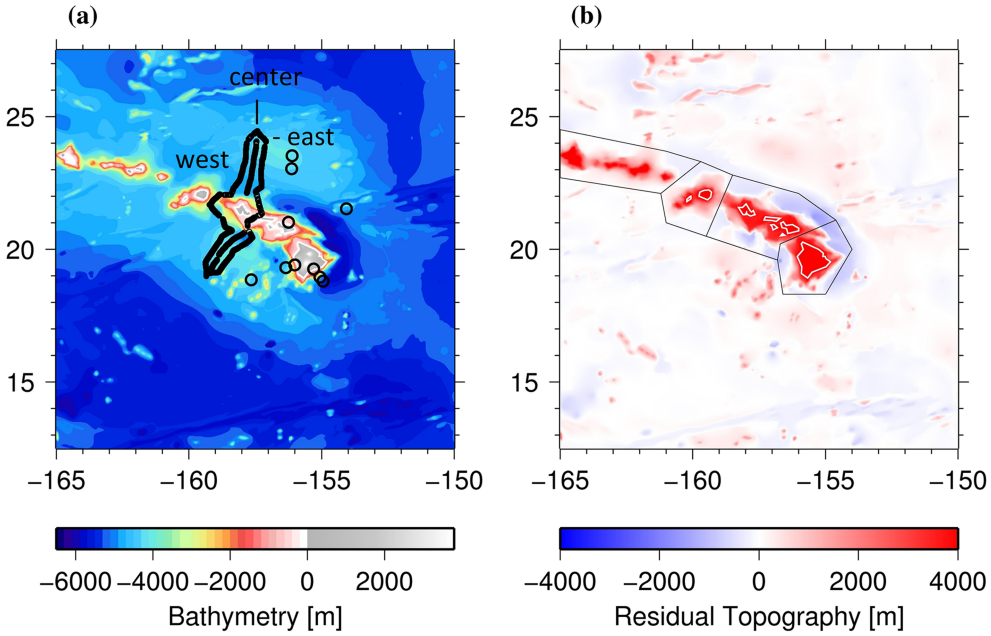

Figure 3. (a) Bathymetry and locations of seismic reflection and refraction data. The data include the three transects which intersect the Hawaiian ridge between Kauai and Oahu and Oahu and Molokai acquired onboard R/V Robert D. Conrad and R/V Kana Keoki in 1982 (Watts et al., 1985). The seismic observations are compared to the model predictions of flexure. (b) The residual topography defines the loads, which are divided into four loading regions (modified from Zhong & Watts, 2013). The residual topography is produced by subtracting the effects of crustal thickness variations, thermal isostasy, and swell topography from the observed bathymetry.

with the depth converted seismic reflection profile data, thus placing constraints on rheology (Zhong & Watts, 2013). We calculate the misfit following Zhong and Watts (2013)

$$\chi = \frac{\sqrt{\Sigma_{i=1}^{N}(M_i - O_i)^2}}{\sqrt{\Sigma_{i=1}^{N} O_i^2}}, \tag{9}$$

where χ is the misfit, M_i is the model flexure at a point, and O_i is the observed deflection at a point. There are more observations of flexure near Oahu and Molokai than at other dispersed locations around the Hawaiian Islands. To make a more complete comparison with the data set, we assign a 50% weight to data in the Kauai-Oahu-Molokai seismic profiles (marked east, center, and west in Figure 3a) and 50% weight to other disparate sites.

For our 3-D Cartesian box of 1,479 km in x (east-west), 1,668 km in y (north-south), and 500 km in z (depth; Figure 2a), we use 32 elements in depth and 128 in each horizontal direction. There is considerable mesh refinement in the upper 50–80 km such that each element spans 5 km in depth. A background asthenospheric viscosity of 10^{20} Pa s is chosen to derive mantle viscosity from high-temperature creep. However, this reference value would lead to a Maxwell time of ~100 years and require an even smaller time step to resolve the viscoelastic deformation. To improve the computational cost by reducing the number of time steps, we impose a lower bound on viscosity of 10^{21} Pa s, thus enabling us to use larger time step Δt in our modeling without affecting stress relaxation in the lithosphere (see Zhong & Watts, 2013). Here we use a constant time step $\Delta t = 0.25\tau_M \sim 250$ years, with the Maxwell timescale τ_M of ~1,000 years corresponding to viscosity of 10^{21} Pa s.

2.2. The Model of Plume-Lithosphere Interaction

To assess the effects of weakening from elevated temperatures in the lithosphere due to a plume, we formulate a convection model to investigate the interaction between the lithosphere and a plume (Figure 2b),

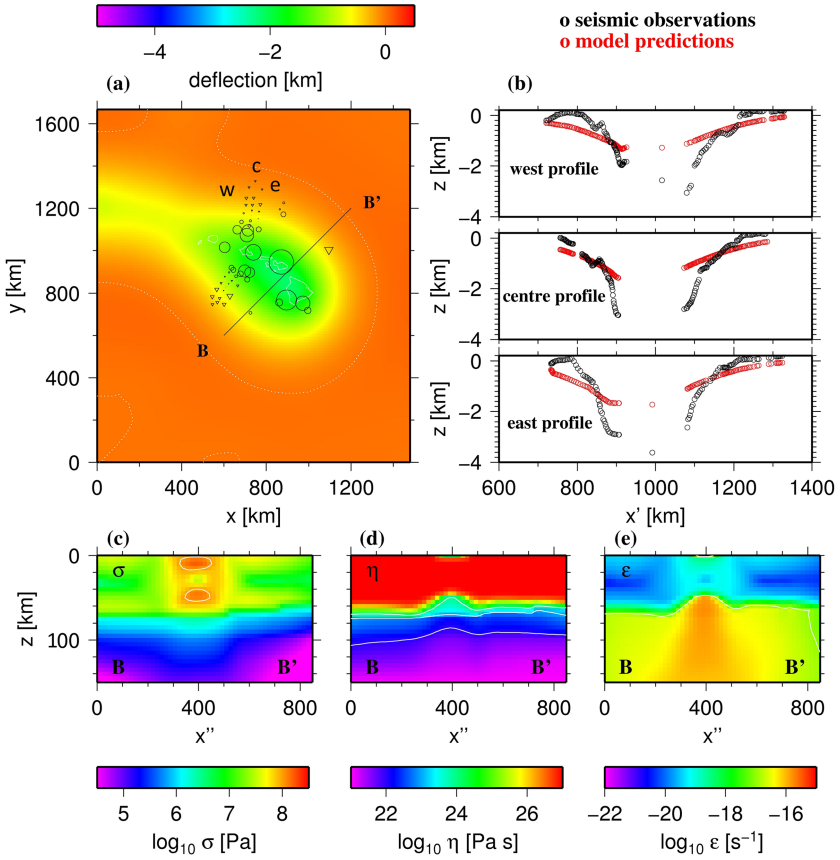

Figure 4. Results from Model 1 with low-temperature plasticity from Idrissi et al. (2016) (Table 2), including (a) the map view of flexure with symbols to show the difference between prediction and observation; circles show underestimation, and triangles show overestimation of flexure. (b) Three cross sections of predicted deflection (red) compared with observations from seismic reflection (black). Finally, the stress (c), viscosity (d), and strain rate (e) along a vertical cross section marked BB′.

which is identical to Zhong and Watts (2002) and similar to Ribe and Christensen (1994). Different from the loading models discussed in the last section, our convection models only consider purely viscous flow with linear, high-temperature creep rheology. Convection models generally ignore elastic, brittle, and low-temperature plastic deformation, which are only relevant for relatively shallow depths (<50 km) to which the plume does not penetrate. The governing equations are the conservation equations of mass, momentum, and energy, and the first two conservation equations are the same as equations (1) and (2), except that the thermal buoyancy (e.g., the plume) is included (e.g., Ribe & Christensen, 1994).

The 3-D box domain is 400 km deep (z), 1,600 km wide (y), and 3,200 km long (x). The plume is simulated by a circular temperature anomaly at the bottom boundary centered at $x = 800$ km and $y = 0$ with a radius of 65 km (Figure 2b). In all cases, the excess temperature of the plume is 300 K. The surface plate motion is fixed to 8.6 cm/year in the x direction, and the initial temperature structure at $x = 0$ is defined by the cooling half-space model at 70 Myr. Conductive cooling occurs as material traverses the domain. The boundary conditions at vertical sidewalls in the x-z plane are free slip (reflecting), while the bottom boundary and vertical sidewalls in the y-z plane are open to perpendicular flow only (material may flow through but there is no slip).

We vary the viscosity contrast across the lithosphere (i.e., the activation energy, E) and the reference asthenospheric viscosity η_0 (Table 2). The steady-state temperature anomaly induced by the plume in the lithosphere is then modeled as a simple functional form and added to the thermal structure in loading models (Table 2). The functional form fits a power law to the plume-induced temperature anomaly at each depth,

Table 2
Model Parameters and Outputs

Plume Model	E (kJ/mol)	η_0 (Pa s)
1p	240	10^{20}
2p	120	10^{20}
3p	120	10^{19}

Viscoelastic Model	LTP flow law	E_p (kJ/mol)	Thermal structure	Misfit
1	Idrissi et al. (2016)	566	HSC	0.507
1a	Idrissi et al. (2016)	400	HSC	0.294
1b	Idrissi et al. (2016)	400	HSC + plume 1p	0.294
1c	Idrissi et al. (2016)	400	HSC + plume 2p	0.294
1d	Idrissi et al. (2016)	400	HSC + plume 3p	0.292
1e	Idrissi et al. (2016)	566	HSC + plume 3p	0.459
1f	Idrissi et al. (2016)	400	Plate model	0.296
1 g	Idrissi et al. (2016)	420	Plate model	0.294
1 h	Idrissi et al. (2016)	566	Plate model	0.445
1i	Idrissi et al. (2016)	400	Plate model + plume 3p	0.297
2	Mei et al. (2010)	320	HSC	0.534
2a	Mei et al. (2010)	190	HSC	0.292
2b	Mei et al. (2010)	320	HSC + plume 3p	0.486
2c	Mei et al. (2010)	320	Plate model	0.476
3	Warren & Hirth (2006)	470	HSC	0.503
3a	Warren & Hirth (2006)	320	HSC	0.299
3b	Warren & Hirth (2006)	470	HSC + plume 3p	0.456
3c	Warren & Hirth (2006)	470	Plate model	0.442
4	Demouchy et al. (2013)	450	HSC	0.446
4a	Demouchy et al. (2013)	350	HSC	0.295
4b	Demouchy et al. (2013)	450	HSC + plume 3p	0.414
4c	Demouchy et al. (2013)	450	Plate model	0.396

Note. HSC stands for half-space cooling.

z, in the x-z plane at $y = 0$ (along the center line of the plume). Then, the temperature perturbation is extrapolated laterally in the y direction to produce the 3-D functional form (see Supporting Information S1).

3. Results

We now present model calculations of volcano-induced flexure for models with various LTP flow laws, activation energy values, and with thermal structures that incorporate the effects of the cooling plate model and the effects of the plume. The model results are compared with the observations of flexure in order to place constraints on individual flow laws. These model calculations represent a significant expansion of the number of test cases and parameters over that of Zhong and Watts (2013).

3.1. New Low-Temperature Plastic Flow Laws and Effect of Activation Energy

In Model 1 (Figure 4), we test a recently published LTP flow law that is weaker compared to others (Idrissi et al., 2016; Kumamoto et al., 2017). It has preexponential factor $A = 1.0 \times 10^6$ s^{-1} MPa^{-1}, stress exponent $n = 1$, activation energy $E_p = 566$ kJ/mol, Peierls stress $\sigma_p = 3.8$ GPa, and exponents p and q are 0.5 and 2, respectively (equation (6) and Table 1). All other parameters in Model 1 are the same as in Zhong and Watts (2013): The frictional coefficient of frictional sliding is 0.7, and the high-temperature creep flow law has activation energy $E_c = 360$ kJ/mol, prefactor η_0=10^{20} Pa s, stress exponent $n = 1$ and $n = 3.5$ in the composite law, and the transition stress $\sigma_{trns} = 0.3$ MPa (Table 1), and the thermal structure is given by the half-space cooling model and local seafloor age.

Model 1 predicts that the amount of surface flexure at present day is broadly 1–2 km with a maximum of 2.1 km located beneath the northwest side of the big island (Figure 4a). The deflection is a long, curved feature that follows the island chain, has a width of approximately 400 km, and narrows in the direction of Pacific

plate motion. Vertical cross sections of the predicted plate surface deflection show the deflection across the island chain at Oahu is <2 km (Figure 4b), and that deflection decreases away from the big island.

Cross sections of stress, viscosity, and strain rate are based on transect BB′ (Figure 4a), which intersects the Hawaiian ridge on the northwest side of the big island. Bending stresses are concentrated in the upper 60 km of the lithosphere with a maximum of ~200 MPa and a local minimum at ~30 km depth which correlates with the neutral surface in the bending plate (Figure 4c). Model 1 predicts a viscosity $>10^{27}$ Pa s in the upper 60 km (i.e., effectively an elastic plate for this high viscosity layer thickness), which decreases to the background viscosity of 10^{21} Pa s for depth ≥150 km (Figure 4d). The apparent thinning at 400 km horizontal distance along BB′ is caused by the local high stress that weakens the lithosphere. Finally, the strain rate in the upper 60 km is ~10^{-20} s^{-1} at 200 km or further from the load, 10^{-19} s^{-1} within 200 km of the load, and 10^{-18} s^{-1} directly beneath the load at shallow depths (Figure 4e). The spatial distribution of strain rate is broadly correlated with that of deflection and stress, all of which exhibit a maximum in a region of width ~400 km centered along the island chain.

The results for Model 1 show significant differences compared to the observations of flexure (Figure 4b). The deflection of the plate is underestimated by up to 2.9 km. More than 100–200 km away from the Hawaiian ridge, flexure is slightly overpredicted, and the predicted deflection pattern is spread over a broader area compared to observation. The normalized root-mean-square (RMS) misfit to flexure data (equation (9)) is 0.507, compared to the optimal misfit of ~0.3 in the best fit models of Zhong and Watts (2013).

In Model 2, we retest a flow law derived in laboratory experiments by Mei et al. (2010) in an exact replica of case R1 in Zhong and Watts (2013). The predicted pattern and amplitude of flexure surrounding the Hawaiian Islands is identical, and the reader is referred to that study for supporting figures. The results of Model 2 are not significantly different from those of Model 1 with a slightly larger misfit to observations of 0.534 (Table 2). In Models 3 and 4, we test the LTP flow law from Warren and Hirth (2006) and Demouchy et al. (2013), respectively (Table 1). The predicted flexure, stress, viscosity, and strain rate are not sufficiently different compared to Models 1 and 2 to warrant additional figures. The misfit of the predicted flexure to observation is 0.503 and 0.446 for Models 3 and 4, respectively (Table 2). In summary, all unmodified LTP flow laws significantly underpredict flexure similarly to Model 1 (Figure 4) and overpredict plate strength for the estimated load and lithospheric thermal structure.

Next, the activation energy of the LTP flow law, E_p, is varied from 566 kJ/mol in Model 1 to 400 kJ/mol in Model 1a, while other parameters are fixed. The plate is broadly flexed by >2 km with a maximum of 4.6 km at $x = 925$ and $y = 821$ km, beneath the big island (Figure 5a). The agreement between prediction and observation is greatly improved along the seismic transects flanking Oahu in Model 1a, although the bulge is not reproduced (Figure 5b). The overall misfit for the flexure is improved from 0.507 (Model 1) to 0.294 (Model 1a). Stresses are concentrated in the upper 40 km, with a local minimum at 20 km (Figure 5c), consistent with the elastic thickness estimate of Watts and ten Brink (1989) and the minimum in observed seismicity (Anchieta et al., 2011; Zhong & Watts, 2013). The predicted viscosity is $>10^{27}$ Pa s in the upper 30–40 km and decreases to the background value 10^{21} Pa s at depths ≥140 km (Figure 5d). The jump in viscosity at ~60 km depth is caused by differences in strength from LTP and high-temperature creep, the latter of which is automatically activated for $T > 800$ °C in the model. The strain rate in the upper 40 km of the lithosphere is ~10^{-20} s^{-1} for lateral distance >200 km from the load and $>10^{-18}$ s^{-1} within 200 km. The strain rate increases to 10^{-15} s^{-1} in the deeper, weaker part of the lithosphere (Figure 5e). The results including the misfit for Model 1a are similar to case R14 of Zhong and Watts (2013), which imposes a weakening factor 10^8 in the preexponential factor of the LTP flow law of Mei et al. (2010).

In Figure 6, the misfit is plotted as a function of the plastic activation energy for each of the flow laws tested in this study. For the Model 1 series, with LTP from Idrissi et al. (2016), the misfit decreases as E_p decreases from 566 (Model 1) to 400 kJ/mol (Model 1a), but the misfit begins to increase for E_p lower than 400 kJ/mol. For E_p less than 400 kJ/mol, the lithosphere becomes too weak and leads to a larger flexure than is observed. The misfit is minimized for the flow law of Model 2 (Mei et al., 2010) when the plastic activation energy, E_p, is reduced from 320 to 190 kJ/mol, for Model 3 (Warren & Hirth, 2006) when it is reduced from 470 to 320 kJ/mol, and for Model 4 (Demouchy et al., 2013) when it is reduced from 450 to 350 kJ/mol (Figure 6). This corresponds to a modest percent reduction in E_p of 26%, 41%, 32%, and 22% relative to laboratory results for Models 1, 2, 3, and 4, respectively. The required degree of weakening from modifying the LTP flow law is not

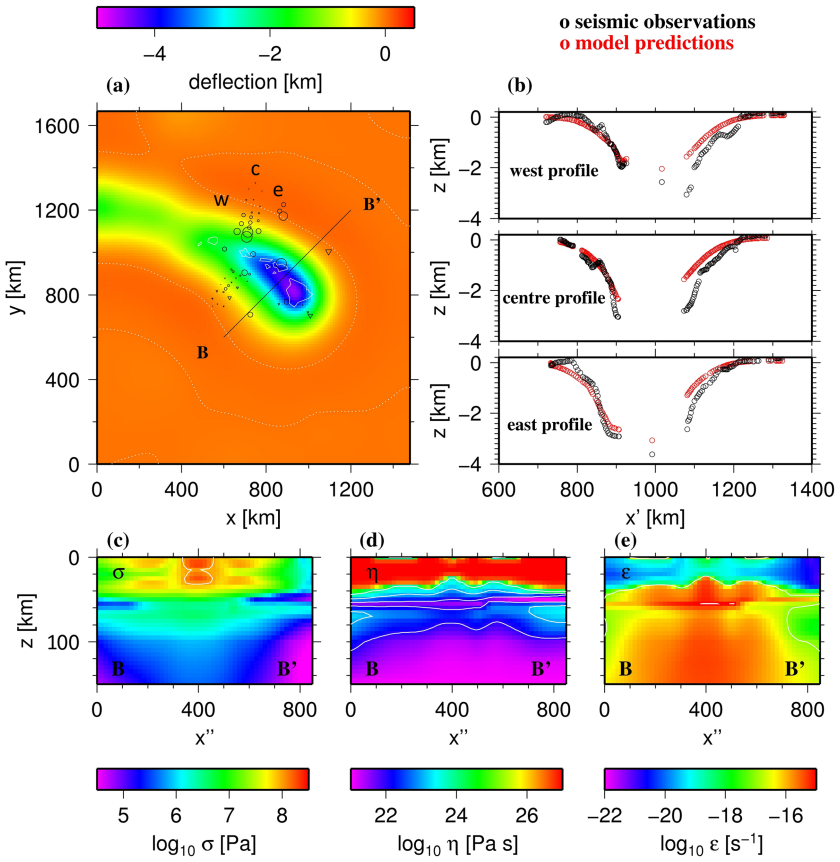

Figure 5. Results for Model 1a with the low-temperature plasticity from Idrissi et al. (2016) with reduced activation energy, E_p, including (a) the map view of predicted deflection with symbols as described in Figure 4, (b) cross sections of predicted deflection (red) compared with observations (black), and finally, stress (c), viscosity (d), and strain rate (e) along a vertical cross section marked BB′.

strongly influenced by high-temperature creep. There is some trade-off with the frictional coefficient, but this effect is also small for $\mu_f \geq 0.25$ which is constrained by the depth of the local minimum in seismicity (Zhong & Watts, 2013).

In Figures 1c and 1d, the stress and strain rate, averaged horizontally within a 250 km radius of Hawaii, are plotted against depth for Models 1 and 1a. The stress is smaller in magnitude but spread over ~60 km depth in Model 1 compared to ~30 km in Model 1a. The strain rate in Model 1 is smaller and exhibits a minimum at ~30 km depth compared to the minimum at ~20 km depth in Model 1a. The strain rate is maximal at, and just below, the base of the high viscosity layer with high stress (i.e., elastic lithosphere), which occurs at ≥60 km depth and ≥30 km in Models 1 and 1a, respectively. The strain rate in Model 1a sharply decreases from $10^{-15.5}$ to $10^{-16.25}$ s^{-1} at 60 km depth where stronger rheology from high-temperature creep is activated by the model setup ($T > 800$ °C). Implications of a depth-dependent strain rate on the yield-strength envelope will be discussed in section 4.

3.2. Effects of Different Lithospheric Thermal Structure

3.2.1. Plume-Induced Thermal Anomalies and Their Effects on Loading-Induced Flexure

We test three plume-lithosphere interaction models that produce varying degrees of thermal erosion in the lithosphere (Table 2). As demonstrated in previous studies (e.g., van Hunen et al., 2005), thermal erosion of the lithosphere by sublithospheric small-scale convection is sensitive to activation energy E of the viscous rheology. The larger E is, the stronger the lithosphere is and the less thermal erosion of the lithosphere occurs. This also applies to thermal erosion of the lithosphere by a plume (e.g., van Hunen & Zhong, 2003). For linear or equivalently Newtonian rheology, which we use here, van Hunen et al. (2005) report that $E = 120$ kJ/mol best reproduces seismic observations of Pacific mantle and lithosphere structure. In plume-

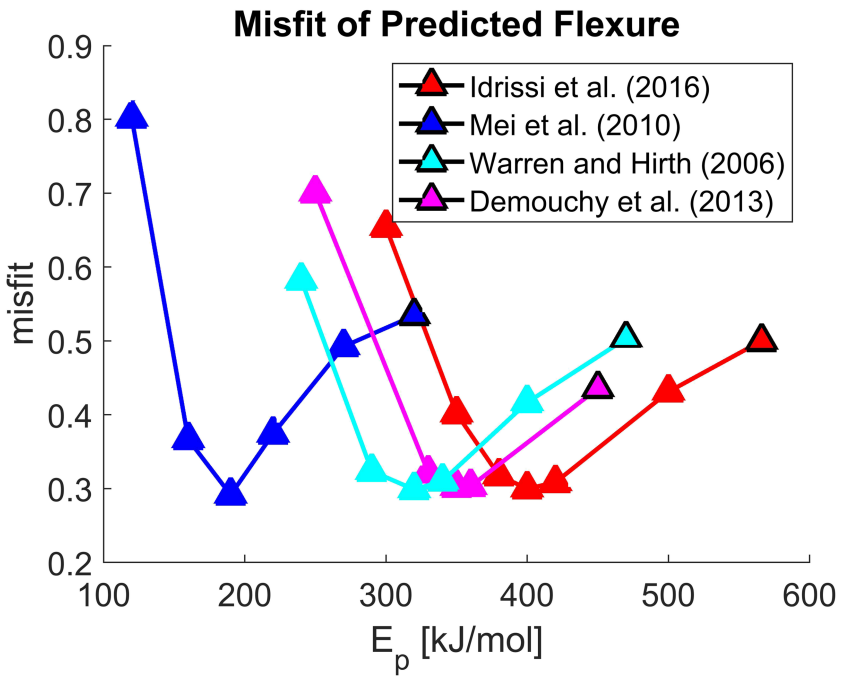

Figure 6. The misfit of predicted to observed flexure as a function of the plastic activation energy, E_p, for various low-temperature plastic flow laws. Symbols outlined in black represent the unmodified activation energy, E_p, published by each laboratory study. Unmodified flow laws produce misfits of 0.446–0.534, but a reduction in plastic activation energy of 26%, 41%, 32%, and 22% reduces the misfit to a minimum value of 0.294, 0.292, 0.299, and 0.295 for Idrissi et al. (2016), Mei et al. (2010), Warren and Hirth (2006), and Demouchy et al. (2013), respectively.

lithosphere interaction models like those in this study, both Ribe and Christensen (1994) and Zhong and Watts (2002) reproduce the Hawaiian swell topography and vertical motion using E of 120–200 kJ/mol. Therefore, in this study we test a range of E = 120–240 kJ/mol. The convection models used herein apply high-temperature creep to the mantle at all depths, as discussed in section 2.2.

Model 1p uses activation energy E = 240 kJ/mol and asthenospheric viscosity $\eta_0 = 10^{20}$ Pa s, which produces the least amount of thermal erosion to the lithosphere among the models we consider. In this case, the temperature perturbation induced by the plume is always less than 50 K in the upper 100 km of the lithosphere (Figure 7a for the cross-sectional temperature perturbation along the center of the plume). The thermal perturbation shallows and diffuses downstream as the buoyant plume material spreads laterally and induces convection at the base of the lithosphere. A temperature perturbation of 10 K reaches a shallowest depth of ~50 km at >2,000 km downstream of the plume conduit, and directly above the plume conduit, it is deeper than 100 km, such that only the deepest portion of the lithosphere is altered.

Model 2p is identical to Model 1p except for the reduction of activation energy from 240 to 120 kJ/mol. Thermal erosion is stronger due to reduced viscosity contrast across the lithosphere, but the pattern is qualitatively similar. The temperature perturbation is always less than 50 K for depth < 60 km (Figure 7b). The 10 K temperature perturbation reaches a shallowest depth of ~30 km at >2,000 km downstream of the plume conduit but is confined to depth > 80 km above the plume. Temperature perturbations of 150 K or more are confined everywhere to depths greater than 100 km.

In Model 3p, we maintain E = 120 kJ/mol and test stronger thermal erosion by reducing viscosity in the asthenosphere η_0 from 10^{20} to 10^{19} Pa s. This case represents the upper limit for plume-induced thermal erosion to the lithosphere based on modeling the plume-lithosphere interaction (Ribe & Christensen, 1994; Zhong & Watts, 2002) and sublithospheric small-scale convection (van Hunen et al., 2005). Reduced asthenospheric viscosity increases the vigor of convection and hence the propensity for thermal erosion. This model develops small-scale convection at the base of the lithosphere that erodes material deeper than 100 km (Figure 7c). The temperature perturbation reaches a maximum value of 600 K at ~100 km depth. A temperature perturbation of 150 K advances from a depth of ~75 km above the plume conduit and to ~25 km at >2,000 km

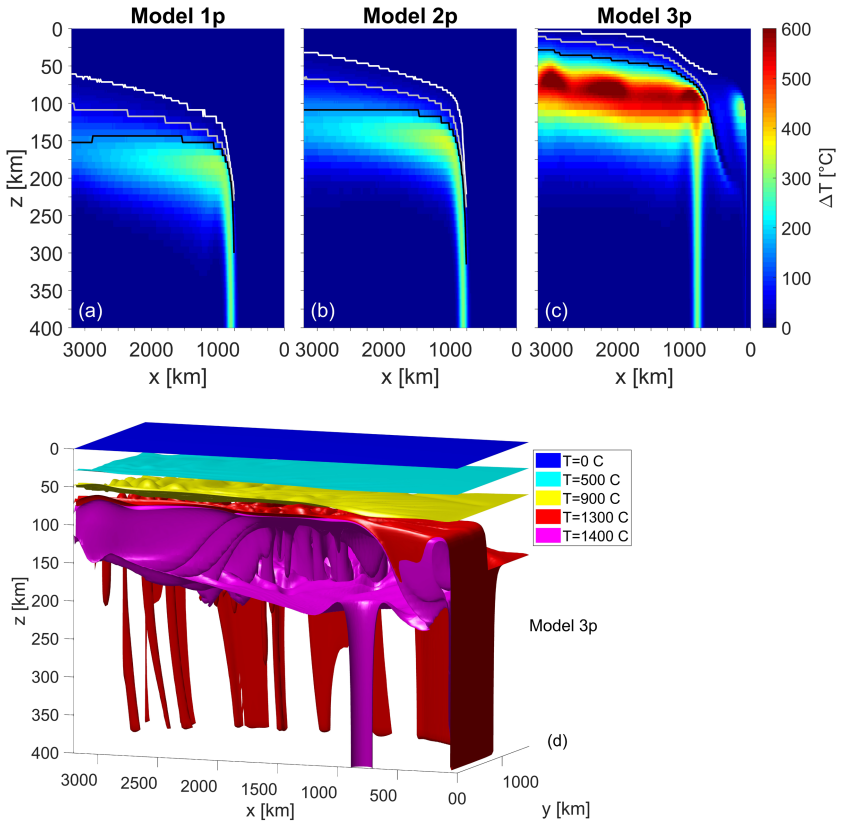

Figure 7. Cross sections along the plume center showing the temperature anomaly from (a) Model 1p with background viscosity $\eta_0 = 10^{20}$ Pa s and activation energy $E_p = 240$ kJ/mol, (b) Model 2p with $\eta_0 = 10^{20}$ Pa s and $E_p = 120$ kJ/mol, and (c) Model 3p with $\eta_0 = 10^{19}$ Pa s and $E_p = 120$ kJ/mol. The contours in (a)–(c) are for temperature anomalies of 10 K (white), 50 K (gray), and 150 K (black). We also show 3-D isotherms from Model 3p (d). The imposed surface velocity of 8.6 cm/year is consistent with Pacific plate motion and in the $+x$ direction (to the left).

downstream from the plume, such that it is confined to large depths within 500 km of the Hawaiian Islands (Figure 7c).

For Model 3p, we also plot quasi-steady state isothermal surfaces in 3-D (Figure 7d). The geotherm is compressed such that the 1300 °C isotherm rises from ~150 to ~100 km depth. The depth of the 900 °C isotherm rises from ~75 to ~50 km at 2,000 km downstream, which is important for understanding its potential effect on the loading calculations, given that LTP is active only for relatively low temperature (e.g., $T < 800$ °C) at shallow depths (<50 km; Figure 5c).

Temperature anomalies advance to shallower depth as pristine 90 Myr old oceanic lithosphere first passes over the plume conduit. As the plate travels downstream with velocity 8.6 cm/year, convective instabilities develop and remove colder, denser material at the base of the lithosphere. Eroded material is replaced with warmer, more buoyant plume material and, together with thermal diffusion, advances the perturbation isotherm to shallower depth.

Although a significant (150 K) temperature perturbation extends to depths as shallow as 25 km at >2,000 km downstream in Model 3p, the observations of flexure with which we compare loading calculation results are confined to within ~500 km distance from the big island of Hawaii. Within this area, the temperature perturbation is everywhere less than 200 K for depth less than 50 km (Figures 7c and S1). In summary, strong ($T > 200$ K) thermal perturbations are confined to the deep lithosphere ($z > 50$ km) in Model 3p, which has the strongest thermal erosion.

Next, we construct a functional form of the temperature perturbation from plume models and add it to loading models. The functional temperature perturbation is a power law in x and y at each depth increment, z.

For more details of plume-lithosphere interaction and the functional form, refer to Supporting Information S1. The temperature anomaly induced by thermal erosion from Model 1p is added to the background temperature structure from a cooling half-space model in Model 1b, which is otherwise identical to Model 1a. The misfit to the observations of flexure is unchanged and equal to 0.294 (Table 2). The maximum deflection is also unchanged and equal to 4.6 km, and the normalized RMS misfit of total deflection (i.e., not only at observation sites) between Models 1a and 1b is 0.0007.

In Model 1c, the temperature anomaly from convection Model 2p is added to the cooling half-space lithospheric thermal structure. The thermal perturbation does not affect the misfit to observation nor the maximum deflection and produces a normalized RMS misfit in deflection of 0.0008 relative to Model 1a. In Model 1d, the temperature anomaly from the strongest plume, Model 3p, is added. The misfit to observations reduces from 0.294 to 0.292, the maximum deflection increases by 130 m, and the normalized RMS misfit with Model 1a is 0.05. The effect of warming the lithosphere by interaction with a plume is therefore modest in models which minimize the misfit to observations (i.e., in Figure 1b with reduced activation energy E_p), even for the strongest thermal erosion reasonable at Hawaii.

The effect of plume anomalies on unmodified LTP flow laws (i.e., in Figure 1a with original activation energy E_p) is also tested. In Model 1e, the temperature anomaly from the strongest plume (Model 3p) is added to Model 1, which uses the unmodified flow law from Idrissi et al. (2016), and background temperature field from the cooling half-space model. The misfit to the observations of flexure reduces from 0.507 in Model 1 to 0.459 in Model 1e, which is a noticeable reduction. For other unmodified LTP flow laws in Models 2–4, adding the temperature anomaly from Model 3p leads to misfit reduction from 0.534 to 0.486, 0.503 to 0.456, and 0.446 to 0.414 in Models 2b, 3b, and 4b, respectively (Table 2). Modification of the thermal structure by a plume has a greater effect on flexure in models with unmodified flow laws than modified flow laws, because lithospheric weakening from a plume is mostly confined to relatively large depth, and unmodified flow laws are otherwise strong at large depth, while modified flow laws are already weakened at depth by the reduction in E_p.

3.2.2. The Effects of the Plate Thermal Model on Loading-Induced Flexure

All loading models tested thus far employ a background thermal structure based on the half-space cooling model. We now test the effect of the plate model's thermal structure on flexure (Stein & Stein, 1992; Turcotte & Schubert, 2002). For a thermal structure defined by the plate model, lithospheric rheology is weakened relative to that with the half-space cooling model, but the weakening is mostly for relatively large depth such that its effect on loading calculations remains small. Model 1f employs the cooling plate model but is otherwise identical to Model 1a with reduced E_p (400 kJ/mol) for the flow law by Idrissi et al. (2016). Model 1f reproduces the observed flexure with misfit of 0.296, compared with Model 1a's misfit of 0.294. The maximum deflection of the plate is 5.4 km, increased by 0.8 km compared to Case 1a, and the normalized RMS misfit of predicted deflection between Models 1a and 1f is 0.11. The larger deflection in Model 1f compared with Model 1a arises because the plate thermal model elevates lithospheric temperature in Model 1f and weakens the lithosphere, relative to Model 1a. The small misfit between Models 1a and 1f suggests large differences in deflection are localized. We find that in Model 1g with E_p increased slightly to 420 KJ/mol but otherwise identical to Model 1f, the misfit to observed flexure decreases to 0.294 (Table 2), which is identical to that for Model 1a, and the maximum deflection is 4.8 km.

The effect of the cooling plate model is also tested with the unmodified flow laws. Model 1h employs the plate thermal model but is otherwise identical to Model 1 which uses the half-space cooling model (i.e., both models use the unmodified flow law of Idrissi et al., 2016). In Model 1h, the maximum flexure increases to 2.7 km compared to 2.1 km, the misfit to observations reduces from 0.507 to 0.445, and the normalized RMS misfit of predicted deflection is 0.16 compared with those from Model 1. Similarly, for other unmodified flow laws in Models 2–4, the plate thermal model reduces the misfit to observations from 0.534 to 0.476, from 0.503 to 0.442, and from 0.446 to 0.396, in Models 2c, 3c, and 4c, respectively (Table 2). This suggests that with the cooling plate model, the lithosphere remains too strong to explain the observed flexure for these unmodified LTP flow laws.

Finally, in Model 1i, we use the modified flow law by Idrissi et al. (2016) with $E_p = 400$ kJ/mol and add to the plate model thermal structure the temperature anomaly associated with the plume of Model 3p (Table 2). The misfit to observations is 0.297 in Model 1i compared to 0.296 in Model 1f, which is identical except

for perturbation by a plume (Table 2). This suggests relatively small influence on flexure from a plume, especially with reduced E_p and the cooling plate model which already weaken the lithosphere at depth > 40 km.

Although weakening from the cooling plate model has a modest effect on flexure, it is a slightly larger effect than that from a plume. This is consistent with temperature anomalies of ~75 °C which extend to depths of ~50 km at Hawaii for the cooling plate model, compared to negligibly small temperature anomaly at depths of ~50 km at Hawaii for thermal erosion from a plume (refer to Supporting Information S1). In addition, using the plate model rather than half-space cooling model has a greater impact on flexure in models with unmodified than modified LTP, such that the misfit to observed flexure may vary by 0.05–0.06 and 0.002 for unmodified and modified LTP rheology, respectively. For comparison, perturbation by a plume produces variation by 0.03–0.05 and 0–0.002 in the misfit to observations for unmodified and modified LTP rheology, respectively. In all cases, perturbing the thermal structure has only a small impact on flexure at Hawaii.

4. Discussion

4.1. Low-Temperature Plasticity

Modeling the observations of flexure in the vicinity of the Hawaiian islands in a nonlinear viscoelastic loading model, Zhong and Watts (2013) found that several published low-temperature plasticity (LTP) flow laws (e.g., Evans & Goetze, 1979; Katayama & Karato, 2008; Mei et al., 2010; Raterron et al., 2004) overpredict lithospheric strength, underpredict the amplitude of flexure, and overpredict the wavelength of flexure. Using similar models, we find that the LTP flow laws of Idrissi et al. (2016), Warren and Hirth (2006), and Demouchy et al. (2013) similarly overestimate lithospheric strength. The misfit to the observations of flexure produced by LTP flow laws of Idrissi et al. (2016), Warren and Hirth (2006), and Demouchy et al. (2013) is 0.507, 0.503, and 0.446, respectively (Figure 6), which is only slightly better than 0.534 using Mei et al. (2010). Although the newly tested flow laws are weaker than previously published ones, the strength they predict in the midlithosphere is still sufficiently large that little or no viscous relaxation of stress occurs, and stresses may be supported elastically on timescales significantly longer than the timescale of Hawaiian Island building.

However, we find that the LTP flow laws may be weakened by a modest reduction of the plastic activation energy, such that the predicted flexure agrees with observations to within a misfit of 0.3. This misfit is consistent with Zhong and Watts (2013), who vary the preexponential factor of the flow laws over 8 orders of magnitude to produce weakening equivalent to that in the present study. We have therefore demonstrated here that variation of plastic activation energy is equally, if not better, suited to calibrate laboratory derived flow laws to field observations. The percent reduction of activation energy required to reproduce flexure at Hawaii is 26%, 41%, 32%, and 22% for Idrissi et al. (2016), Mei et al. (2010), Warren and Hirth (2006), and Demouchy et al. (2013), respectively. We must emphasize that flexure alone cannot constrain the plastic activation energy alone, because it is coupled to other parameters in the flow law. Rather, we constrain the depth-dependent yield-strength envelope, which must be consistent with the observations of flexure.

The flow law of Mei et al. (2010) produces the strongest yield-strength envelope (Figure 1a) and largest misfit and requires the greatest reduction in activation energy out of all LTP flow laws tested in this study. In contrast, the low-temperature plastic flow law from Demouchy et al. (2013) predicts a stronger yield-strength envelope than Idrissi et al. (2016), but a smaller misfit, and the least variation in activation energy to reproduce observed flexure. We suggest that this apparent role reversal is attributed to a difference in the conditions imposed for the yield-strength envelope inversion ($\dot{\varepsilon} = 10^{-16}\,\mathrm{s}^{-1}$, age of the seafloor = 90 Ma) and those in the Hawaiian region ($\dot{\varepsilon}$ and σ vary in 3-D, and age of the seafloor varies in 2-D). Taking this into account, at least in the region of the Hawaiian Islands, Demouchy et al. (2013) predicts the weakest rheology of all LTP flow laws tested herein and is, therefore, most consistent with the observations of flexure.

Our loading model results for strain rate and stress vary with depth (Figures 1c and 1d) and have implications for the yield strength envelope. To determine the yield strength envelope (e.g., Figure 1), a strain rate must be specified to solve the yield stress from the deformation mechanisms and corresponding flow laws relevant to the lithosphere. Typically, the strain rate is assumed constant for simplicity. However, our loading models show that strain rate may vary by more than 2 orders of magnitude in the top 40 km of the lithosphere (Figures 1d, 4e, and 5e and Zhong & Watts, 2013). We investigate the effect of depth-dependent strain

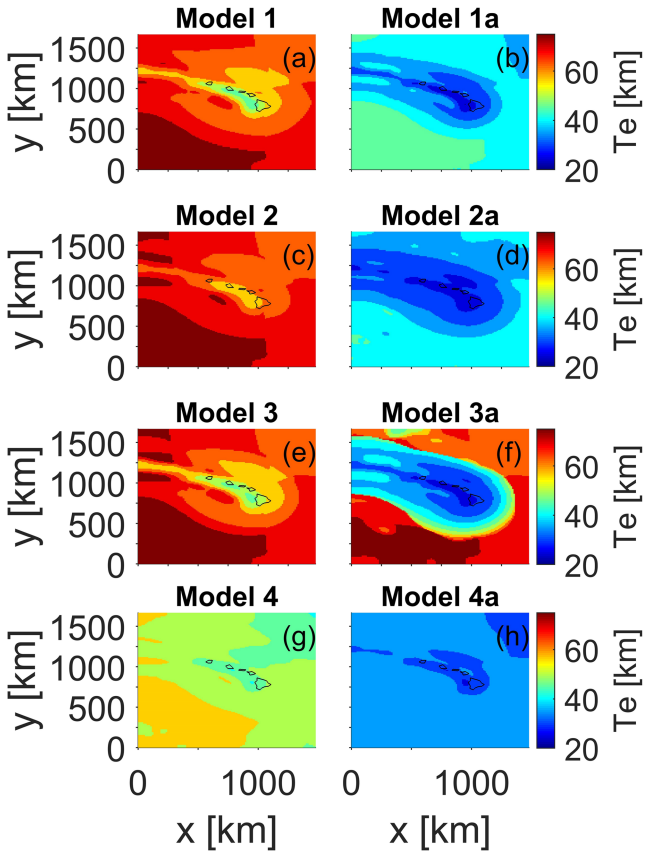

Figure 8. The equivalent elastic thickness estimates from Models 1 to 4 with unmodified flow laws (a, c, e, g) and (b, d, f, h) Models 1a–4a with modified flow laws (Table 2). The equivalent elastic thickness is the thickness of the layer with viscosity exceeding 10^{26} Pa s. The average elastic thickness predicted in the region which undergoes flexure is 62 km (a, c, e, g) or 33 km (b, d, f, h).

rate on the yield-strength envelope using the strain rate profile in Figure 1 d from Model 1a. The depth-varying strain rate introduces relatively small differences in the strength envelope for most of the flow laws, except in the modified flow law of Mei et al. (2010), which is reduced by nearly a factor of two at intersection with the Goetze criterion (Figures 1b and 1f). The yield-strength envelopes predicted by weakened-LTP (i.e., in Models 1a, 2a, 3a, and 4a) are in relatively good agreement with one another compared to unmodified flow laws, regardless of whether constant or depth-dependent strain rate is imposed (Figure 1). Additionally, it is evident that lithospheric stress from dynamic loading models (e.g., Figure 1c) can differ significantly from the yield strength envelope. The yield strength envelope only sets an upper limit on the stress, while the true lithospheric stress in regions subject to loads from volcanoes may be significantly less and must follow the laws of continuum mechanics (i.e., conservation of mass and momentum), which has implications for estimates of elastic thickness from the yield-strength envelope method (Burov & Diament, 1995; Hunter & Watts, 2016).

A major motivation behind geodynamic modeling studies, such as this one, is to test and verify the rheological strength of the lithosphere as it ultimately pertains to the development of plate tectonics. Laboratory-derived flow laws consistently predict that the lithosphere is too strong for plate tectonics to emerge dynamically on Earth (Davaille & Limare, 2015; Moresi & Solomatov, 1998). Extensive work has developed a theory of dynamic weakening in high-temperature creep (Bercovici & Ricard, 2016), which reduces the high strength of the lithosphere in localized regions and produces features resembling plate boundaries. However, it seems that the LTP rheology, which appears to govern the strongest portion of the lithosphere (Figures 1a and 1b), may also play an important role in generating plate tectonics. Recent studies in mineral physics suggest that the LTP deformation mechanism may strengthen in regions that undergo large amounts of strain and grain-size reduction (Hansen et al., 2019; Kumamoto et al., 2017), such as plate boundaries, which we suggest may complicate an understanding of how to initiate and maintain plate tectonics. Similarly, Hunter and Watts (2016) report that laboratory flow laws for LTP fit the observations of flexure at subduction zones but are too strong at the Hawaiian Islands. Building an understanding of LTP in the plate interiors, and how it evolves at plate boundaries, will be a critical aspect of understanding plate tectonics on Earth and other planets. This study represents an important step in constraining the LTP rheology by using the observations of flexure at the Hawaiian Islands.

4.2. Elastic Thickness

The rheology of the lithosphere is not that of an ideal elastic plate, despite the success of such a model in explaining a wide range of geological phenomena. Elastic thickness is a proxy for the integrated strength and may be used with some confidence to compare relative weakness and rigidity of the lithosphere (Billen & Gurnis, 2005; Burov & Diament, 1995). Viscosities greater than 10^{26} Pa s corresponds to a Maxwell time $\tau_M \geq 100$ Myr, such that the lithosphere is essentially elastic on the timescale of Hawaiian volcano emplacement ($\leq$5 Myr). The high-viscosity layer supports stresses elastically and limits deformation. We use can therefore use this criterion to estimate an effective elastic thickness and draw comparisons with previous studies of lithospheric flexure.

The viscosity exceeds 10^{26} Pa s to an average depth of 65, 68, 66, and 50 km in Models 1, 2, 3, and 4, respectively, and 33, 32, 32, and 34 km in corresponding weakened (via reducing the low-temperature plastic activation energy) Models 1a, 2a, 3a, and 4a, respectively (Figure 8). The misfit to the observations of flexure ranges from ~0.45 to 0.55 for Models 1–4, which is reduced to ~0.3 for Models 1a–4a with modest reduction in plasticity activation energy. The inferred elastic thickness based on modeling gravity anomalies and

flexure in a purely elastic plate model is 33 km at Hawaii (Wessel, 1993) or 30 km for the Hawaiian Islands (Zhong & Watts, 2013), which is consistent with estimates of elastic thickness for 90 Ma lithosphere at other intraplate locations (Watts & Zhong, 2000). This consistency in elastic thickness estimates suggests that the lithosphere at Hawaii is a good representation of oceanic lithosphere for its age and is not anomalous in either its thermal or mechanical structure, a conclusion that is corroborated by seismic studies (Ritzwoller et al., 2004; Woods et al., 1991), and measurements of surface heat flow (von Herzen et al., 1989).

4.3. Effect of a Plume on Flexure

The strong influence of thermal structure on lithospheric strength suggests thermal rejuvenation by a plume could bring laboratory-derived flow laws into agreement with geophysical observation and modeling. However, we have shown that the viscosity contrast across the lithosphere is such that it prevents a plume from significantly modifying the thermal structure above 50 km depth beneath the Hawaiian Islands. The time dependence of thermal convection constrains shallower thermal perturbations to large distances downstream of the plume conduit. The effect of a plume-induced thermal structure on flexure is small because significant temperature perturbations are confined to the deep lithosphere, where the rheology is already relatively weak and does little to support stress from volcanic loads such as those that make up the Hawaiian Islands. Any appreciable modification of the thermal structure must, therefore, be highly localized (Guest et al., 2018) or confined to very large distances downstream of the plume conduit (Pleus et al., 2018).

In a purely hypothetical test, the perturbation to lithospheric thermal structure required to reduce the misfit from 0.507 to 0.328 for the unmodified LTP flow law of Idrissi et al. (2016) is equivalent to a uniform age reduction by 50 Myr. However, such extensive thermal rejuvenation of lithosphere beneath the Hawaiian Islands is inconsistent with seismic observations and the lack of heat flow and elastic thickness anomalies in the region and is not supported by our convection models of plume-lithosphere interaction. Therefore, we conclude that the laboratory-derived LTP flow laws underestimate the flexure not because of thermal rejuvenation from a plume but rather because they are too strong compared to conditions in the real Earth. However, our study also demonstrates that these LTP flow laws can be made consistent with the observations by a modest (by 25–40%) reduction in plasticity activation energy, suggesting the importance of laboratory studies exploring uncertainties in rheological parameters including activation energy (Jain et al., 2017).

5. Conclusions

By comparing the seismically constrained observations of flexure at the Hawaiian Islands to the calculated flexure of a 3-D loading model with a realistic nonlinear rheology, we test the applicability of the experimentally derived LTP flow laws of Demouchy et al. (2013), Idrissi et al. (2016), and Warren and Hirth (2006) to lithospheric conditions. We have also examined the effects of thermal perturbations by a plume, and from different conductive cooling models, on lithospheric strength and flexure. Our results can be summarized as follows.

1. The LTP flow laws of Demouchy et al. (2013), Idrissi et al. (2016), and Warren and Hirth (2006) in their original forms significantly overpredict lithospheric strength at Hawaii and underpredict the lithospheric flexure relative to the observed. However, these LTP flow laws can be weakened to reproduce flexure at Hawaii if the plastic activation energy, E_p, is reduced by 25–40%.
2. The thermal structure defined by the plate model has an insignificant effect on lithospheric flexure at the Hawaiian Islands, compared with the thermal structure of a cooling half-space model. Also, the Hawaiian mantle plume does not appear to produce any significant thermal perturbation to the top 50 km of the lithosphere in the vicinity of the Hawaiian Islands, such that the influence of plume-induced thermal perturbation on flexure is negligible.

Acknowledgments
We are thankful for constructive feedback from Dr. G. Ito and an anonymous reviewer. We also thank Dr. Ito for sharing his manuscript, Pleus et al. (in review), after submission of the present study. This work is supported by grants from NASA ESI 80NSSC18K0470 and NSF EAR-1940026 without which this work would not be possible. Data are available online (https://doi.org/10.6084/m9.figshare.10295477).

References

Anchieta, M. C., Wolfe, C. J., Pavlis, G. L., Vernon, F. L., Eakins, J. A., Solomon, S. C., et al. (2011). Seismicity around the Hawaiian Islands Recorded by the PLUME Seismometer Networks: Insight into faulting near Maui, Molokai, and Oahu. *BSSA*, *101*(4), 1742–1758.

Ballmer, M. D., Ito, G., Wolfe, C. J., & Solomon, S. C. (2013). Double layering of a thermochemical plume in the upper mantle beneath Hawaii, Earth Planet. *Science Letters*, *376*, 155–164. https://doi.org/10.1016/j.epsl.2013.06.022

Bercovici, D., & Ricard, Y. (2016). Grain-damage hysteresis and plate-tectonic states. *Physics of the Earth and Planetary Interiors*, *253*, 31–47.

Billen, M. I., & Gurnis, M. (2005). Constraints on subducting plate strength within the Kermadec trench. *Journal of Geophysical Research*, *110*, B05407. https://doi.org/10.1029/2004JB003308

Burov, E. B., & Diament, M. (1995). The effective elastic thickness (T_e) of continental lithosphere: what does it really mean? *Journal of Geophysical Research*, *100*, 3905–3927.

Byerlee, J. (1978). *Friction of rocks, Pageoph* (Vol. 116). Basel: Birkhauser Verlag.

Davaille, A., & Limare, A. (2015). Laboratory studies of mantle convection. *Treatise of Geophysics*, *7*, 73–144.

Demouchy, S., Tommasi, A., Boffa Ballaran, T., & Cordier, P. (2013). Low strength of Earth's uppermost mantle inferred from tri-axial deformation experiments on dry olivine crystals. *Physics of the Earth and Planetary Interiors*, *220*, 37–49.

Detrick, R. S., & Crough, S. T. (1978). Island subsidence, hot spots, and lithospheric thinning. *Journal of Geophysical Research*, *83*, 1236–1244.

Evans, B., & Goetze, C. (1979). The temperature variation of hardness of olivine and its implication for polycrystalline yield stress. *Journal of Geophysical Research*, *84*, 5505–5524.

Freed, A. M., Herring, T., & Bürgmann, R. (2010). Steady-state laboratory flow laws alone fail to explain post-seismic observations, Earth Planet. *Science Letters*, *300*, 1–10.

Guest, I., Garcia, M., Ito, G., & Hellebrand, E. (2018). Rapid thermal rejuvenation under O'ahu inferred from Salt Lake Crater garnet pyroxenite xenoliths, Abstract MR43C-0118 presented at 2018 Fall Meeting, AGU, Washington, D.C., 10-14 Dec.

Hager, B. H., & Richards, M. A. (1989). Long-wavelength variations in Earth's geoid: Physical models and dynamical implications. *Philosophical Transactions of the Royal Society A*, *328*, 309–327.

Hansen, L. N., Kumamoto, K. M., Thom, C. A., Wallis, D., Durham, W. B., Goldsby, D. L., et al. (2019). Low-temperature plasticity in olivine: Grain size, strain hardening, and the strength of the lithosphere. *Journal of Geophysical Research. Solid Earth*, *124*, 5427–5449. https://doi.org/10.1029/2018JB016736

Hunter, J., & Watts, A. B. (2016). Gravity anomalies, flexure and mantle rheology seaward of circum-Pacific trenches. *Geophysical Journal International*, *207*, 288–316.

Idrissi, H., Bollinger, C., Boioli, F., Schryvers, D., & Cordier, P. (2016). Low-temperature plasticity of olivine revisited with in situ TEM nanomechanical testing. *Science Advances*, *2*(3), e1501671. https://doi.org/10.1126/sciadv.1501671

Jain, C., Korenaga, J., & Karato, S.-I. (2017). On the yield strength of oceanic lithosphere. *Geophysical Research Letters*, *44*, 9716–9722. https://doi.org/10.1002/2017GL075043

Katayama, I., & Karato, S.-I. (2008). Low-temperature, high-stress deformation of olivine under water-saturated conditions. *Physics of the Earth and Planetary Interiors*, *168*, 125–133.

Kohlstedt, D. L., Evans, B., & Mackwell, S. J. (1995). Strength of the lithosphere: Constraints imposed by laboratory experiments. *Journal of Geophysical Research*, *100*, 17,587–17,602.

Kohlstedt, D. L., & Mackwell, S. J.(2009). Strength and deformation of planetary lithospheres. In *Planetary Tectonics* (pp. 397–456). Cambridge University Press.

Kumamoto, K. M., Thom, C. A., Wallis, D., Hansen, L. N., Armstrong, D. E. J., Warren, J. M., et al. (2017). Size effects resolve discrepancies in 40 years of work on low-temperature plasticity in olivine. *Science Advances*, *3*(9), e1701338. https://doi.org/10.1126/sciadv.1701338

Mei, S., Suzuki, A. M., Kohlstedt, D. L., Dixon, N. A., & Durham, W. B. (2010). Experimental constraints on the strength of the lithospheric mantle. *Journal of Geophysical Research*, *115*(B8), B08204. https://doi.org/10.1029/2009JB006873

Moresi, L., & Solomatov, S. (1998). Mantle convection with a brittle lithosphere: Thoughts on the global tectonic styles of the Earth and Venus. *Geophysical Journal International*, *133*(3), 669–682. https://doi.org/10.1046/j.1365-246X.1998.00521.x

Parsons, B., & Sclater, J. G. (1977). An analysis of the variation of ocean floor bathymetry and heat flow with age. *Journal of Geophysical Research*, *82*(5), 803–827. https://doi.org/10.1029/JB082i005p00803

Peltier, W. R. (1976). Glacial isostatic adjustment: II. The inverse problem. *Geophysical Journal of the Royal Astronomical Society*, *46*, 669–705.

Pleus, A., Ito, G., Wessel, P., & Frazer, L. N. (2018). *In situ* rheology of the oceanic lithosphere along the Hawaiian Ridge, Abstract T23E-0419 presented at 2018 Fall Meeting. Washington, D.C.: AGU. 10-14 Dec

Raterron, P., Wu, Y., Weidner, D. J., & Chen, J. (2004). Low-temperature olivine rheology at high pressure. *Physics of the Earth and Planetary Interiors*, *145*, 149–159.

Ribe, N. M., & Christensen, U. R. (1994). 3-Dimensional modeling of plume-lithosphere interaction. *Journal of Geophysical Research*, *99*, 669–682.

Ritzwoller, M. H., Shapiro, N. M., & Zhong, S. J. (2004). Cooling history of the Pacific lithosphere, Earth Planet. *Science Letters*, *226*, 69–84.

Shor, G. G., & Pollard, D. D. (1964). Mohole site selection studies north of Maui. *Journal of Geophysical Research*, *69*, 1627–1637.

Sibson, R. H. (1974). Frictional constraints on thrust, wrench and normal faults. *Nature*, *249*.

Stein, C. A., & Stein, S. (1992). A model for the global variation in oceanic depth and heat flow with lithospheric age. *Nature*, *359*, 123–129.

Turcotte, D. L., & G. Schubert (2002). *Geodynamics* (2nd ed., 456 p.). New York: Cambridge University Press.

van Hunen, J., Zhong, S., Shapiro, N. M., & Ritzwoller, M. H. (2005). New evidence for dislocation creep from 3-D geodynamic modeling the Pacific upper mantle structure. *Earth and Planetary Science Letters*, *238*, 146–155.

van Hunen, J., & Zhong, S. J. (2003). New insight in the Hawaiian plume swell dynamics from scaling laws. *Geophysical Research Letters*, *30*(15), 1785. https://doi.org/10.1029/2003GL017646

von Herzen, R. P., Cordery, M. J., Detrick, R. S., & Fang, C. (1989). Heat flow and the thermal origin of hot spot swells: The Hawaiian swell revisited. *Journal of Geophysical Research*, *94*, 783–799.

Warren, J. M., & Hirth, G. (2006). Grain size sensitive deformation mechanisms in naturally deformed peridotites. *Earth and Planetary Science Letters*, *248*, 438–450.

Watts, A. B., ten Brink, U., Buhl, P., & Brocher, T. (1985). A multichannel seismic study of lithospheric flexure across the Hawaiian-Emperor seamount chain. *Nature*, *315*, 105–111.

Watts, A. B., & ten Brink, U. S. (1989). Crustal structure, flexure, and subsidence history of the Hawaiian Islands. *Journal of Geophysical Research*, *94*(B8), 10,473–10,500.

Watts, A. B., & Zhong, S. J. (2000). Observations of flexure and the rheology of oceanic lithosphere. *Geophysical Journal International*, *142*, 855–875.

Wessel, P. (1993). A reexamination of the flexural deformation beneath the Hawaiian Islands. *Journal of Geophysical Research*, *98*, 12,177–12,190.

Woods, M. T., Leveque, J.-J., Okal, E. A., & Cara, M. (1991). Two-station measurement of Rayleigh wave group velocity along the Hawaiian swell. *Geophysical Research Letters*, *18*, 105–108.

Wu, P. (1992). Deformation of an incompressible viscoelastic flat earth with power-law creep: A finite-element approach. *Geophysical Journal International*, *108*(1), 35–51.

Zhong, S. J., Paulson, A., & Wahr, J. (2003). Three-dimensional finite element modeling of Earth's viscoelastic deformation: Effects of lateral variations in lithospheric thickness. *Geophysical Journal International*, *155*, 679–695.

Zhong, S. J., & Watts, A. B. (2002). Constraints on the dynamics of mantle plumes from uplift of the Hawaiian Islands. *Earth and Planetary Science Letters*, *203*, 105–116.

Zhong, S. J., & Watts, A. B. (2013). Lithospheric deformation induced by loading of the Hawaiian Islands and its implications for mantle rheology. *Journal of Geophysical Research: Solid Earth*, *118*, 6025–6048. https://doi.org/10.1002/2013JB010408

Zhong, S. J., Zhang, N., Li, Z. X., & Roberts, J. H. (2007). Supercontinent cycles, true polar wander, and very long-wavelength mantle convection. *Earth and Planetary Science Letters*, *261*, 551–564.

Zoback, M. D., & Townend, J. (2001). Implications of hydrostatic pore pressures and high crustal strength for the deformation of intraplate lithosphere. *Tectonophysics*, *336*, 19–30.

Zucca, J. J., & Hill, D. P. (1980). Crustal structure of the southeast flank of Kilauea volcano, Hawaii, from seismic refraction measurements. *Bulletin of the Seismological Society of America*, *70*, 1149–1159.

Zucca, J. J., Hill, D. P., & Kovach, R. L. (1982). Crustal structure of Mauna Loa Volcano, Hawaii, from seismic refraction and gravity data. *Bulletin of the Seismological Society of America*, *72*, 1535–1550.